Applied Physics Letters

Multiple scattering in scanning helium microscopy

Cite as: Appl. Phys. Lett. **116**, 061601 (2020); https://doi.org/10.1063/1.5143950
Submitted: 31 December 2019 . Accepted: 28 January 2020 . Published Online: 10 February 2020

S. M. Lambrick, L. Vozdecký, M. Bergin, J. E. Halpin, D. A. MacLaren, P. C. Dastoor, S. A. Przyborski, A. P. Jardine, and D. J. Ward

Applied Physics Letters ARTICLE scitation.org/journal/apl

Multiple scattering in scanning helium microscopy

Cite as: Appl. Phys. Lett. **116**, 061601 (2020); doi: 10.1063/1.5143950
Submitted: 31 December 2019 · Accepted: 28 January 2020 ·
Published Online: 10 February 2020

S. M. Lambrick,[1,a)] L. Vozdecký,[1] M. Bergin,[1] J. E. Halpin,[2] D. A. MacLaren,[2] P. C. Dastoor,[3] S. A. Przyborski,[4] A. P. Jardine,[1] and D. J. Ward[1]

AFFILIATIONS

[1]Department of Physics, Cavendish Laboratory, University of Cambridge, JJ Thomson Avenue, Cambridge CB3 0HE, United Kingdom
[2]SUPA, School of Physics and Astronomy, University of Glasgow, Glasgow G12 8QQ, United Kingdom
[3]Centre for Organic Electronics, Physics Building, University of Newcastle, Callaghan NSW 2308, Australia
[4]Department of Biosciences, Durham University, South Road, Durham DH1 3LE, United Kingdom

[a)]Author to whom correspondence should be addressed: sml59@cam.ac.uk

ABSTRACT

Using atom beams to image the surface of samples in real space is an emerging technique that delivers unique contrast from delicate samples. Here, we explore the contrast that arises from multiple scattering of helium atoms, a specific process that plays an important role in forming topographic contrast in scanning helium microscopy (SHeM) images. A test sample consisting of a series of trenches of varying depths was prepared by ion beam milling. SHeM images of shallow trenches (depth/width < 1) exhibited the established contrast associated with masking of the illuminating atom beam. The size of the masks was used to estimate the trench depths and showed good agreement with the known values. In contrast, deep trenches (depth/width > 1) exhibited an enhanced intensity. The scattered helium signal was modeled analytically and simulated numerically using Monte Carlo ray tracing. Both approaches gave excellent agreement with the experimental data and confirmed that the enhancement was due to localization of scattered helium atoms due to multiple scattering. The results were used to interpret SHeM images of a bio-technologically relevant sample with a deep porous structure, highlighting the relevance of multiple scattering in SHeM image interpretation.

Scanning helium microscopy (SHeM) is a nascent technology that scans a narrow beam of low energy neutral helium atoms over a surface, to produce images of materials without any possibility of beam damage.[1–4] The technique can be applied widely and has particular applications in imaging delicate samples, which are difficult to measure using existing techniques.[5] Examples include the imaging of insulators, polymers, and biological materials, all of which can be done without coatings or other preparation. As the technique becomes used more broadly, it is crucial to have a good understanding of the image formation process. Here, we report on the significant role that multiple scattering plays in the contrast observed in SHeM images. We use a test sample with simple, well defined, topography. By comparing experimental images with quantitative contrast modeling, we obtain a clear understanding of the process. We also show how quantitative topographic information can be extracted without making any assumptions about the atom-surface interaction. These insights are then used to understand and interpret helium images of a bio-technologically relevant sample in its native state.

Contrast in scanning helium microscopy has similarities with the origins of contrast in scanning electron microscopy, both of which involve rastering a focused or collimated beam across the sample and the collection of a fraction of the backscattered signal. In the case of helium atoms, a narrow spot can be generated via simple pinhole collimation, as used in the current work;[3] via diffractive focusing with a Fresnel zone plate or similar;[6–8] or through the use of atom mirrors.[9–12] Since the local surface position and orientation affect the resulting distribution of scattered particles, topographic contrast is evident in both cases. The scattering geometries mean that images appear as if they are illuminated from the direction of the detector, and when a point on the sample is occluded from the detector, typically by a convex region of sample structure, "masked" regions are formed in the image. However, there are also significant differences between the

angular distributions of scattered electrons and helium atoms, due to the underlying differences in interaction with surfaces,[13] and the different relative detector sizes; helium detectors only cover a relatively small fraction of solid angle. These issues have a significant effect on contrast formation and image interpretation.

In current SHeM instruments, the incident beam is typically at 45° to the sample normal and illuminates a small region on the surface, corresponding to a particular pixel in the image. Atoms scattered through a total angle of approximately 90° reach the detector and are counted to give the pixel intensity. There are three primary contributions to topographic contrast, which have been discussed in the literature and are useful to distinguish here. First, height contrast arises primarily from a change in the proportion of the scattered signal that is detected using a fixed position detector;[14,15] however, such contrast is weak and only appears over large changes in the height.[14–16] Second, angular orientation contrast[14,16] occurs when the local orientation of the sample changes the portion of the scattering distribution that enters the detector aperture. For the largely diffuse scattering that occurs from unprepared surfaces, higher intensity is expected when the local surface is orientated toward the detector. Finally, masking, due to the detector being occluded from the illuminated spot on the sample, gives very strong contrast as primary scattered atoms cannot be detected. Masking is independent of the atom-surface interaction[14–17] but is related to the underlying surface topography, thus enabling quantitative topographic information to be extracted.

A particularly important feature of SHeM is that since there is essentially no possibility of sample penetration by, or adsorption of, the probe particles, incident helium atoms can undergo multiple scattering. Given atoms travel along straight line paths, there is a limited probability of them reaching the detector entrance aperture after a single scattering event (~0.5% in our current arrangement). However, by scattering from the sample multiple times, atoms can reach the detector indirectly, and thus, multiple scattering makes a further contribution to topographic contrast. We also note that multiple scattering can also provide weak diffuse illumination, a process that has been previously noted[15,17] but not examined in detail.

A SHeM image of our test sample is shown in Fig. 1, along with its corresponding surface profile. The sample consists of a set of trenches (manufactured by plasma focused ion beam milling of a silicon wafer), each with the same area but different depths. Measured depths of some of the trenches are given in Table I. The helium image clearly shows a distinction between the "shallow" trenches on the right hand side of the image, exhibiting dark regions that widen with the depth, and "deep" trenches on the left hand side of the image, showing very similar, almost uniform, contrast without distinct dark regions. The transition from shallow to deep trenches occurs at a depth/width ratio of about 1. The deep trenches appear significantly brighter than the dark regions in the shallow trenches. Looking closely, the intensity inside the deep trenches increases from left to right, and on the inside right, it even exceeds the intensity of the flat substrate.

The observed contrast in the shallow trenches arises as there is a region of the base of the trench that is masked from the detector (i.e., no line of sight) by the trailing edge of the trench. Masking manifests as the dark region that extends from left to right across the trench and increases with the trench depth. Where the trenches become deeper than they are wide, they become completely masked, which, given the SHeM geometry used, occurs at a depth/width ratio of 1. However, at this point, their appearance also changes, indicating a different explanation is required. We will show that where there are large depth/width ratios, and hence confined spaces, multiple scattering of helium is dominant since the numerous surfaces that are close to each other act to redirect atoms toward the detector. These multiple scattering processes may therefore be thought of as localization of the gas in the trenches.

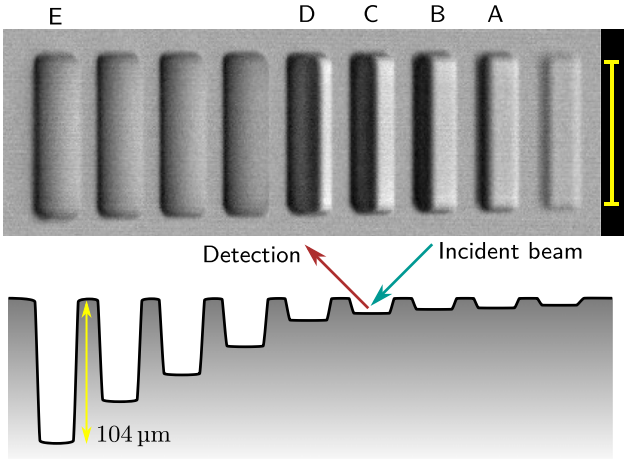

FIG. 1. SHeM image of the test sample with the corresponding surface profile. The helium beam is incident from the right as shown, while the detector is located to the left. As a result of re-deposition during ion beam milling, the sides of the trenches are not vertical and edges of the trenches are rounded. The scale bar length is 100 μm. See the supplementary material for further details.

To investigate multiple scattering contrast, an analytical model was developed. As illustrated in Fig. 2, when atoms enter deep trenches, only a fraction of the singly scattered atoms leave the trench without scattering again. The helium atoms that remain in the trench form a localized gas, which undergoes multiple scattering events, thus randomizing their trajectories. The multiply scattered atoms eventually emerge from the trench diffusely, with a broad distribution of directions, a proportion of which reaches the detector. The total multiple scattered intensity that emerges from inside a trench is dependent on the proportion of atoms that remain localized after the first scattering event. Assuming a cosine model to be representative of diffuse scattering from these "unprepared" surfaces,[18,19] we can calculate the proportion of helium atoms that escape on first scattering. From Fig. 2, it is found that if the beam is incident at a distance, d, into an infinitely

TABLE I. Measured depth of the trenches with a SHeM image, found by measuring the sizes of masks in the image and from an optical profiling microscope. Note that the uncertainty in SHeM mostly arises from the size of pixels used and is similar to the resolution of the instrument. The values agree to within error.

Trench	SHeM/μm	Optical profiler/μm
A	7 ± 2	7.6 ± 0.2
B	10 ± 2	11.1 ± 0.2
C	13 ± 2	14.8 ± 0.3
D	16 ± 2	18.7 ± 0.4

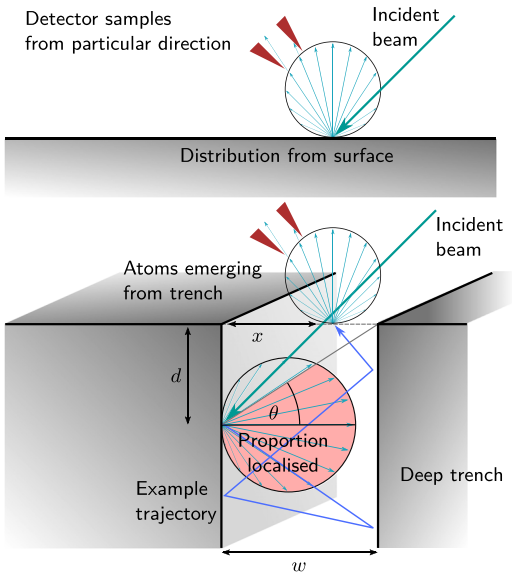

FIG. 2. Top: unprepared surfaces typically scatter with a diffuse distribution. The distant detector, indicated by red triangles, samples part of that distribution in a particular direction. Bottom: atoms falling a long distance, *d*, into a deep trench of width, *w*, become localized, losing memory of their original trajectory. When they escape the trench, they leave with a diffuse distribution that is again sampled in a particular direction by the detector. As the same part of the distribution is sampled, the trench gives the same signal as the flat surface, scaled by the fraction localized. *x* is the raster position.

deep and long trench with width w, then the localized proportion as a function of the ratio d/w is

$$P\left(\frac{d}{w}\right) = \underbrace{\frac{1}{2}\int_0^{\arctan\frac{d}{w}} \cos\theta\,\mathrm{d}\theta}_{\text{Top half of distribution}} + \underbrace{\frac{1}{2}\int_0^{\frac{\pi}{2}} \cos\theta\,\mathrm{d}\theta}_{\substack{\text{Bottom half of distribution}\\ \text{all stays in trench}}}, \tag{1}$$

$$= \frac{1}{2}\sin\left(\arctan\frac{d}{w}\right) + \frac{1}{2} = \frac{1}{2}\left(1 + \frac{d}{\sqrt{d^2 + w^2}}\right). \tag{2}$$

The above 2D result is shown to be mathematically equivalent to the full 3D integral in the supplementary material. In the SHeM, samples are scanned under the beam, and so with lateral movement, the beam falls a different distance into each trench, and thus, the variable d in Eq. (2) may be directly replaced with the lateral position across the trench, x,

$$P(x) = \frac{1}{2}\left(1 + \frac{x}{\sqrt{x^2 + w^2}}\right). \tag{3}$$

Equation (3) gives the proportion of the incident beam that is localized. If the scattering distribution from the surface and the distribution emanating from the trench are exactly the same, then the detected signal will be equal to the proportion localized. However, this also implies that the signal detected from the trench could never exceed the signal from a flat region of the sample, which is not consistent with Fig. 1. Thus, we must consider the case of a different distribution being produced by the localized gas. The detector in the SHeM, as indicated by the red detector apertures in Fig. 2, samples a fixed proportion of the scattering distribution. The detected intensity as a function of x can therefore be written as

$$I(x) = m(\boldsymbol{\xi})\,P(x), \tag{4}$$

where $m(\boldsymbol{\xi})$ gives the probability of detection of the localized gas distribution relative to the surface scattering distribution for some source and detector geometry denoted $\boldsymbol{\xi}$. In the case of the test sample, $\boldsymbol{\xi}$ is constant across the image, and in general, it is fixed for a single image feature.

To further understand which elements of the observed contrast are due to multiple scattering and which are from single scattering, Monte Carlo (MC) ray tracing was used to simulate micrographs of the test sample[15] and to separate the primary and multiply scattered components of the image. The procedure involves tracing straight line paths of atoms as they scatter off the sample and local machine environment. The method requires a model for the scattering distribution from the surface; here, a cosine distribution was used, which is representative of largely diffuse scattering.[18,19]

The top panel of Fig. 3 shows a comparison of the experimental data with both the analytical model and the simulated ray tracing model with and without multiple scattering. In the case of the analytical model, it was found that a value of $m = 1.3$ was in good agreement with the experimental data, and moreover, since the value of m is greater than 1, it implies the multiply scattered atoms are being weakly "beamed" toward the detector (see the supplementary material for further discussion). In Fig. 3, the simulated ray tracing images for the shallow trench (right hand panels) show that although the dominant masking feature is reproduced by primary scattering, including multiple scattering improves the agreement by increasing the intensity on the right hand side of the trench. As with shadows observed with light, the sizes of masks are dependent on the sizes of the features casting them, and thus, the images of the shallow trenches offer the potential for gaining quantitative topographic information from an interaction independent contrast mechanism. In the current setup, a single image was taken, which does not allow for a complete reconstruction, but given our knowledge that the sample consists of trenches with steep sides, an estimation of the depth can be obtained from the masked SHeM images. These depth measurements are comparable well with the trench depths measured using an optical profiling microscope, given in Table I.

In contrast to the shallow trench images, the helium signal observed experimentally for deep trenches (left hand in each pair of images in Fig. 3) is only seen in the simulated images that include multiple scattering (on the top right of Fig. 3), with primary scattered rays producing a fully masked dark image. A quantitative comparison of the intensity variation across the deep trenches is given in the lower panel of Fig. 3, which plots line scans across the experimental, analytical, and simulated deep trench helium images. There is very good quantitative agreement between the experimental and MC multiple scattering simulations, confirming that the observed deep trench helium contrast does indeed originate from multiple scattering of the incident helium atoms. There is also good quantitative agreement between the experimental and analytical line scan data with the fitted value of m. Both models exhibit the same shape across the inside of the trench, but break down near the edges where the topography is more complicated.

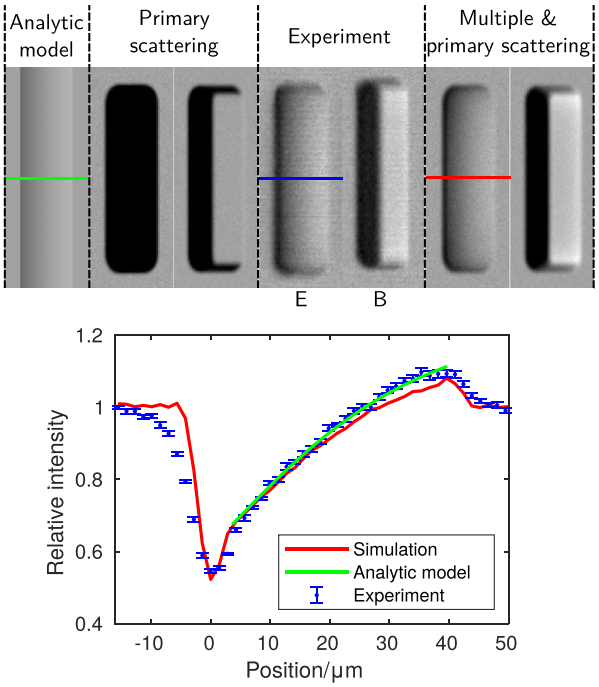

FIG. 3. Top: comparison between the experimental and simulated images of deep and shallow trenches with depth/width ratios of 3.5 and 0.3, respectively. Primary and multiple scattering contributions are shown separately, to the left and right of the experimental images. Once multiple scattering is included, the simulation matches the experimental data closely, with only a slight discrepancy at the edges of the trench where the exact curvature is unknown. It can also be noted that the primary scattering image of the deep trench is symmetric, while the multiple scattering image is not, and thus, the multiple scattering contrast is adding information about the orientation of the trench, with respect to the scattering geometry, which is not present with only primary scattering. Bottom: line scans extracted from experimental and simulated data along with the analytical model from Eq. (4). The analytical model with a value of $m = 1.3$ predicts the direction and form of the intensity change and matches the experimental data well.

An understanding of multiple scattering effects, and how they manifest in contrast, is of particular importance for SHeM imaging of a wide range of surfaces and interfaces of technological interest. As a case study example, porous scaffolds are used extensively in biomedical sciences for growing tissue samples. These scaffolds are constructed out of delicate insulating materials and, as such, have proved to be challenging to image in electron microscopy without degradation or a conductive coating.[20] The non-destructive nature of the neutral SHeM incident atom beam enables the imaging of tissue scaffolds in their native state, allowing tissue growth on exactly the same scaffold as has been imaged.

A disk of Alvetex™, with a nominal pore diameter of 42 μm, was imaged in the SHeM. Alvetex is a cross-linked form of porous polystyrene, manufactured using a method known as emulsion templating involving the formation of a polyHIPE (high internal phase emulsion). The material is used as a scaffold for a large number of applications in 3D cell culture and tissue modeling—notably the formation of skin.[21,22] The pores in the scaffold are akin to the high aspect ratio trenches discussed earlier; helium gas enters the pores and has no direct line of sight to the detector, but localization in the pores

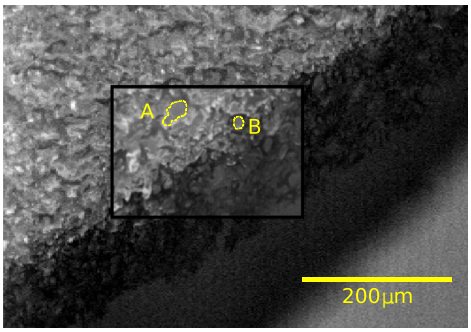

FIG. 4. Helium images of the edge of the Alvetex scaffold. The inset shows the image at a higher pixel density. Regions A and B denote two scaffold pore regions, one in the flat region of the sample and the second along the edge of the sample, which demonstrate a mid-level of the signal compared to the bright and dark scaffold material.

results in multiple scattering and hence an enhanced probability of reaching the detector. A difference with the model trenches is the very high depth of the pores in Alvetex, regardless of the angle of the incident beam to them; behind the surface pores is a complex structure of large voids and further pores. Therefore, there is no significant change in the proportion of the incident beam localized across the pores, and the beam always strikes surfaces a long way into the structure and not near the surface. As there is no change in localization across the pores, the intensity across them is expected to be roughly constant. Figure 4 shows a helium image taken of the Alvetex scaffold. The structure can be seen as either light, when pointing toward the detector, or dark, when pointing away from the detector. The voids in the pores appear gray rather than dark (regions A and B) as expected from our localization model, highlighting the importance of a detailed understanding of multiple scattering.

In summary, multiple scattering is an important topographical contrast mechanism in the SHeM. It is driven by the fact that the ultra-low energy helium atoms scatter exclusively from the surface topography with negligible probability of adsorption or penetration. We have shown that multiple scattering contrast can be understood both qualitatively and quantitatively using analytical modeling and Monte Carlo ray tracing. These studies show that for shallow features, primary scattering dominates, producing topographic contrast that is controlled by surface masks, which can be used to estimate the depths of the surface features. In contrast, for deep features, multiple scattering dominates, producing enhanced contrast within the trench or void. The transition between shallow and deep features occurs at a depth/width ratio of 1, which is defined by the 45° scattering geometry of the instrument. Finally, we have shown that multiple scattering within high aspect ratio voids or pores is an important contrast generation process in technologically relevant samples such as biological scaffolds.

See the supplementary material for further experimental details, an evaluation of the full 3D version of Eq. (1), and a consideration of the implications of the value of the coefficient, m. A dataset supporting this work is published at https://doi.org/10.17863/CAM.48316.

CN Technical Services Ltd. and Dr. Z. Chang provided line profiles of the stepped sample using a KLA Zeta-20 Optical Profiler.

This work was supported by EPSRC Grant Nos. EP/R008272/1 and EP/R008051/1. S.M.L. acknowledges funding from Mathworks Ltd. P.C.D. gratefully acknowledges support from The Leverhulme Trust for the provision of a Leverhulme Visiting Professorship.

REFERENCES

[1]M. Koch, S. Rehbein, G. Schmahl, T. Reisinger, G. Bracco, W. E. Ernst, and B. Holst, J. Microsc. **229**, 1 (2008).
[2]P. Witham and E. Sánchez, Rev. Sci. Instrum. **82**, 103705 (2011).
[3]P. Witham and E. Sánchez, "Nuclear instruments and methods in physics research section B: beam interactions with materials and atoms," in 20th International Workshop on Inelastic Ion-Surface Collisions (IISC-20) (2014), Vol. 340, p. 76.
[4]D. MacLaren and W. Allison, Inst. Phys. Conf. Ser. **179**, 383 (2004).
[5]T. A. Myles, S. D. Eder, M. G. Barr, A. Fahy, J. Martens, and P. C. Dastoor, Sci. Rep. **9**, 2148 (2019).
[6]S. D. Eder, X. Guo, T. Kaltenbacher, M. M. Greve, M. Kalläne, L. Kipp, and B. Holst, Phys. Rev. A **91**, 043608 (2015).
[7]S. D. Eder, T. Reisinger, M. M. Greve, G. Bracco, and B. Holst, New J. Phys. **14**, 073014 (2012).
[8]R. Flatabø, S. D. Eder, A. K. Ravn, B. Samelin, M. M. Greve, T. Reisinger, and B. Holst, Rev. Sci. Instrum. **89**, 053702 (2018).
[9]B. Holst and W. Allison, Nature **390**, 244 (1997).
[10]D. Barredo, F. Calleja, P. Nieto, J. J. Hinarejos, G. Laurent, A. L. V. d Parga, D. Farías, and R. Miranda, Adv. Mater. **20**, 3492 (2008).
[11]A. Politano, B. Borca, M. Minniti, J. J. Hinarejos, A. L. Vázquez de Parga, D. Farías, and R. Miranda, Phys. Rev. B **84**, 035450 (2011).
[12]K. Fladischer, H. Reingruber, T. Reisinger, V. Mayrhofer, W. E. Ernst, A. E. Ross, D. A. MacLaren, W. Allison, D. Litwin, J. Galas, S. Sitarek, P. Nieto, D. Barredo, D. Farías, R. Miranda, B. Surma, A. Miros, B. Piatkowski, E. Søndergård, and B. Holst, New J. Phys. **12**, 033018 (2010).
[13]D. Farias and K.-H. Rieder, Rep. Prog. Phys. **61**, 1575 (1998).
[14]M. Bergin, "Instrumentation and contrast mechanisms in scanning helium microscopy," Ph.D. thesis (Fitzwilliam College, University of Cambridge, 2018).
[15]S. Lambrick, M. Bergin, A. Jardine, and D. Ward, Micron **113**, 61 (2018).
[16]A. Fahy, S. Eder, M. Barr, J. Martens, T. Myles, and P. Dastoor, Ultramicroscopy **192**, 7 (2018).
[17]P. Witham and E. Sánchez, Cryst. Res. Technol. **49**, 690 (2014).
[18]M. Knudsen, *The Kinetic Theory of Gases: Some Modern Aspects*, 3rd ed. (Methuen, London, 1950).
[19]D. R. O'Keefe and R. L. Palmer, J. Vac. Sci. Technol. **8**, 27 (1971).
[20]M. Vielreicher, S. Schürmann, R. Detsch, M. A. Schmidt, A. Buttgereit, A. Boccaccini, and O. Friedrich, J. R. Soc. Interface **10**, 20130263 (2013).
[21]D. S. Hill, N. D. P. Robinson, M. P. Caley, M. Chen, E. A. O'Toole, J. L. Armstrong, S. Przyborski, and P. E. Lovat, Mol. Cancer Ther. **14**, 2665 (2015).
[22]M. Roger, N. Fullard, L. Costello, S. Bradbury, E. Markiewicz, S. O'Reilly, N. Darling, P. Ritchie, A. Määttä, I. Karakesisoglou, G. Nelson, T. V. Zglinicki, T. Dicolandrea, R. Isfort, C. Bascom, and S. Przyborski, J. Anat. **234**, 438 (2019).